

$(0.22^{+0.14}_{-0.16}) \times 10^{-8}$ cm³/s, respectively. The plateau in the $^2\Pi_{1/2g}$ rate and the peak in the $^2\Pi_{3/2g}$ rate (Fig. 3) are caused by increasing Franck-Condon overlap between the $v = 0$ wave function and the continuum vibrational wave function in the $^1\Sigma_u^+$ dissociative channel as the electron energy increases. Dividing these rate constants by the total experimental DR rate constant (22) from $v = 0$ of $2.0 \times 10^{-7} \times (T_e/300)^{-0.65}$ cm³/s gives the quantum yields for O(¹S). For $^2\Pi_{1/2g}$, these yields are $0.020^{+0.015}_{-0.010}$ at $T_e = 300$ K and 0.029 ± 0.003 at $T_e = 800$ K. For a 300 K ion temperature (including only the $^2\Pi_{1/2g}$ and $^2\Pi_{3/2g}$ $v = 0$ levels) and $T_e = 300$ K, the quantum yield is $0.016^{+0.013}_{-0.008}$. At an 800 K ion temperature and $T_e = 800$ K, the quantum yield is $0.026^{+0.007}_{-0.008}$.

The calculated yields at 800 K fall within the 0.01 to 0.23 range of yields derived from atmospheric measurements. The rate coefficients reported here are in good agreement with those derived from plasma spectroscopy measurements (23) (Fig. 3), in which the effective vibrational temperatures indicate that between 67 and 85% of the ions are in $v = 0$ (24). Queffelec *et al.* (25) have reported a quantum yield for $v = 0$ of 0.1 from a flowing afterglow experiment in which the O₂⁺ ions were in $v \leq 2$. However, their experiment has high plasma densities (6) at which the recombination is dominated by processes other than two-body DR. A charge transfer experiment (26) that generates O₂ high Rydberg states and detects dissociation products gave a quantum yield for O(¹S) from $v = 0$ of 0.033, similar to the result reported here. A recent heavy-ion storage ring experiment (27) reported a quantum yield of 0.05 ± 0.02 , also in agreement with my result.

REFERENCES AND NOTES

- M. B. McElroy, *Science* **175**, 443 (1972); J. L. Fox, *Geophys. Res. Lett.* **20**, 1747 (1993); M. H. G. Zhang, J. G. Luhmann, S. W. Bougher, A. F. Nagy, *J. Geophys. Res.* **98**, 10915 (1993).
- J. L. Fox, *Adv. Space Res.* **10** (no. 5), 31 (1990); A. F. Nagy and T. E. Cravens, *Geophys. Res. Lett.* **15**, 433 (1988).
- D. R. Bates, in *Applied Atomic Collision Physics*, vol. 1, H. S. W. Massey and D. R. Bates, Eds. (Academic Press, New York, 1982), pp. 149–224.
- M. B. McElroy, M. J. Prather, J. M. Rodriguez, *Science* **215**, 1614 (1982).
- J. E. Frederick *et al.*, *J. Geophys. Res.* **81**, 3923 (1976); P. B. Hays and W. E. Sharp, *ibid.* **78**, 1153 (1973); H. Takahashi *et al.*, *Planet. Space Sci.* **38**, 547 (1990).
- D. R. Bates, *Planet. Space Sci.* **38**, 889 (1990).
- V. J. Abreu, S. C. Solomon, W. E. Sharp, P. B. Hays, *J. Geophys. Res.* **88**, 4140 (1983).
- S. L. Guberman, *Nature* **327**, 408 (1987).
- _____ and A. Giusti-Suzor, *J. Chem. Phys.* **95**, 2602 (1991).
- D. R. Bates, *Planet. Space Sci.* **40**, 893 (1992).
- S. L. Guberman, in *Physics of Ion-Ion and Electron-Ion Collisions*, F. Brouillard and J. W. McGowan, Eds. (Plenum, New York, 1983), pp. 167–200.

- D. R. Bates, *Phys. Rev.* **78**, 492 (1950).
- J. N. Bardsley, *J. Phys. B* **1**, 365 (1968).
- H. Lefebvre-Brion and R. W. Field, *Perturbations in the Spectra of Diatomic Molecules* (Academic Press, Orlando, FL, 1986).
- The spin-orbit splitting used here was rounded off from the reported value of 200.33 cm⁻¹ for $v = 0$. See E. A. Colbourn and A. E. Douglas, *J. Mol. Spectrosc.* **65**, 332 (1977).
- T. H. Dunning Jr., *J. Chem. Phys.* **90**, 1007 (1989).
- H.-J. Werner and P. J. Knowles, *ibid.* **82**, 5053 (1985); P. J. Knowles and H.-J. Werner, *Chem. Phys. Lett.* **115**, 259 (1985).
- H.-J. Werner and P. J. Knowles, *J. Chem. Phys.* **89**, 5803 (1988); P. J. Knowles and H.-J. Werner, *Chem. Phys. Lett.* **145**, 514 (1988).
- For $^3\Sigma_u^-$, the differences between the calculated and experimental values (28) for the fundamental frequency, the equilibrium internuclear separation, and the excitation energy are 12 cm⁻¹, 0.0006 a₀, and 0.0642 eV, respectively. For $^1\Sigma_u^+$ and O₂ + X² Π_g , the excitation energy differences are 0.06 eV (29) and 0.1636 eV (28), respectively. These energy differences are accounted for in the rate coefficient uncertainties.
- MOLPRO is a package of ab initio programs written by H.-J. Werner and P. J. Knowles, with contributions from J. Almlöf, R. D. Amos, M. J. O. Deegan, S. T. Elbert, C. Hampel, W. Meyer, K. Peterson, R. Pitzer, A. J. Stone, P. R. Taylor, and R. Lindh. Contact molpro-request@tc.bham.ac.uk
- A. Giusti, *J. Phys. B* **13**, 3867 (1980).
- P. Spanel, L. Dittrichova, D. Smith, *Int. J. Mass Spectrom. Ion Processes* **129**, 183 (1993).
- E. C. Zipf, *Planet. Space Sci.* **36**, 621 (1988).
- _____, *J. Geophys. Res.* **85**, 4232 (1980).
- J. L. Queffelec, B. R. Rowe, F. Vallee, J. C. Gomet, M. Morlais, *J. Chem. Phys.* **91**, 5335 (1989).
- H. Helm, I. Hazell, C. W. Walter, P. C. Cosby, in *Dissociative Recombination: Theory, Experiment, and Applications*, D. Zaffman, J. B. A. Mitchell, D. Schwalm, B. R. Rowe, Eds. (World Scientific, Singapore, 1996), pp. 139–150.
- D. Kella, L. Vejby-Christensen, P. J. Johnson, H. B. Pedersen, L. H. Andersen, *Science* **276**, 1530 (1997); *ibid.* **277**, 167 (1997).
- K. P. Huber and G. Herzberg, *Molecular Spectra and Molecular Structure, IV. Constants of Diatomic Molecules* (Van Nostrand Reinhold, New York, 1979); P. H. Kruperie, *J. Phys. Chem. Ref. Data* **1**, 423 (1972).
- B. R. Lewis *et al.*, *Phys. Rev. A* **52**, 2717 (1995).
- Supported by NASA grants NAG5-4316 and NAG5-4286 and NSF grant ATM-9503224.

27 June 1997; accepted 7 October 1997

Mantle Fluids in the San Andreas Fault System, California

B. M. Kennedy, Y. K. Kharaka, W. C. Evans, A. Ellwood, D. J. DePaolo, J. Thordsen, G. Ambats, R. H. Mariner

Fluids associated with the San Andreas and companion faults in central and south-central California have high ³He/⁴He ratios. The lack of correlation between helium isotopes and fluid chemistry or local geology requires that fluids enter the fault system from the mantle. Mantle fluids passing through the ductile lower crust must enter the brittle fault zone at or near lithostatic pressures; estimates of fluid flux based on helium isotopes suggest that they may thus contribute directly to fault-weakening high-fluid pressures at seismogenic depths.

The San Andreas fault (SAF) is known to be a weak fault, and explanations for its weakness include either low-friction fault-zone materials or superhydrostatic fluid pressures within the fault zone (1–3). Abnormally high fluid pressures have been measured in pores at shallow crustal depths within the SAF system (4). For example, fluid pressure in the Varian–Phillips well, 1.4 km from the main trace of the SAF, is ~12 MPa over hydrostatic values at a depth of 1.5 km (5).

Models of fault weakening by elevated fluid pressures call on different fluid origins. Crustal fluids, connate or meteoric, may be

drawn into the fault zone in response to fault rupture and become trapped by mineral reactions; the high fluid pressures required to weaken the fault are reestablished by compaction of the sealed fault-zone materials (6–8). In this model, the base of the seismogenic zone, defined by the brittle-ductile transition, is treated as an impermeable boundary. In an alternative model, fault-weakening fluid pressures are generated by a high flux of deep crustal or mantle fluids that are continually supplied to the seismogenic zone from the ductile lower crust at superhydrostatic pressures (9).

To investigate fluid source and influence on SAF dynamics, we conducted a chemical and helium isotopic study of selected springs, seeps, and wells associated with the SAF and companion faults. Elevated discharge temperatures or salinity, unusual solute chemistry, high gas or water flow rates, or other indications of deep circulation or extensive water-rock interaction were used to select sampling sites. We found that the

B. M. Kennedy, Center for Isotope Geochemistry, Lawrence Berkeley National Laboratory, Berkeley, CA 94720, USA.

Y. K. Kharaka, W. C. Evans, J. Thordsen, G. Ambats, R. H. Mariner, Water Resources Division, U.S. Geological Survey, Menlo Park, CA 94025, USA.

A. Ellwood and D. J. DePaolo, Center for Isotope Geochemistry, Geology and Geophysics Department, University of California, and Lawrence Berkeley National Laboratory, Berkeley, CA 94720–4767, USA.

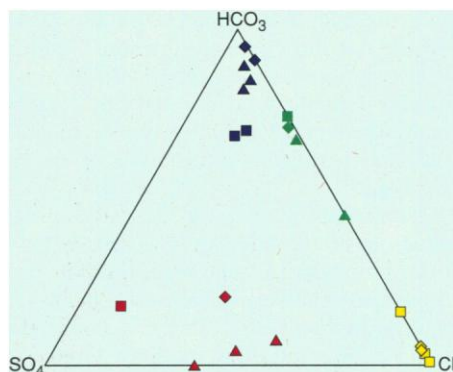


Fig. 1. Ternary plot of major anion concentrations in deep fault-zone fluids from the San Andreas system. Covariations delineate four chemically distinct fluids: chloride-rich (yellow), sulfate-rich (red), bicarbonate-rich (blue), and bicarbonate- and chloride-rich (green). The range in total dissolved solids is 260 mg/liter for some of the bicarbonate fluids to 46,800 mg/liter for the chloride-rich brines. Symbol shapes refer to sample groups defined by location: San Andreas Group (SAG, squares), western Transverse Ranges (SYG, triangles), and the southern Coast Ranges (CRG, diamonds).

fluids can be divided into four categories based on geochemistry (Fig. 1) and into meteoric or evolved connate based on water isotopes (Fig. 2).

Fluids enriched in crustal helium are characterized by a $^3\text{He}/^4\text{He}$ ratio of ~ 0.02 Ra, whereas mantle helium has a value of ~ 8 Ra (Ra is the $^3\text{He}/^4\text{He}$ ratio in air, 1.4×10^{-6}) (10). The helium isotopic compositions in our samples varied from 0.12 to 4.0 Ra (11) and indicate that fluids associated with the SAF system contain mantle He contributions of ~ 1 to $\sim 50\%$ (Fig. 3). Mantle helium occurs throughout the entire investigated segment of the SAF (Fig.

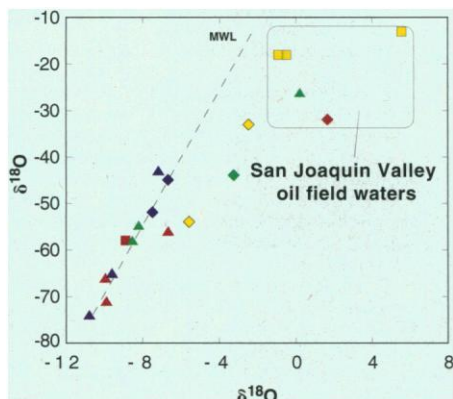
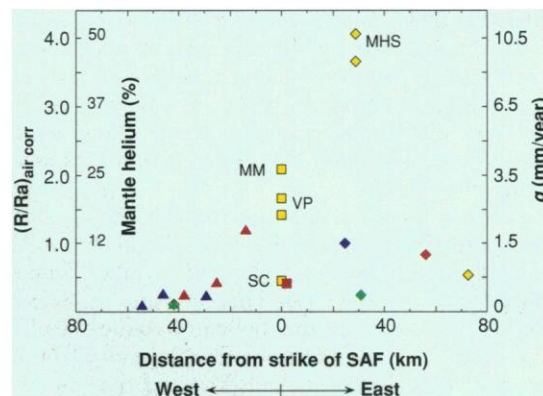


Fig. 2. Isotopic composition of fault-zone waters (symbols as in Fig. 1). Dashed line labeled MWL (meteoric water line) depicts expected variations in the isotopic composition of meteoric waters. Box defines the range in isotopic compositions of oil field waters from the San Joaquin Valley, California (31).

Fig. 3. Helium isotopic composition plotted as a function of approximate distance from the main strike of the SAF (symbols as in Fig. 1: MHS, Mercey Hot Spring; MM, Middle Mountain Oil Well; VP, Varian-Phillips Well; SC, Stone Canyon Well). Associated flow rates and mantle contributions are calculated as described in text.

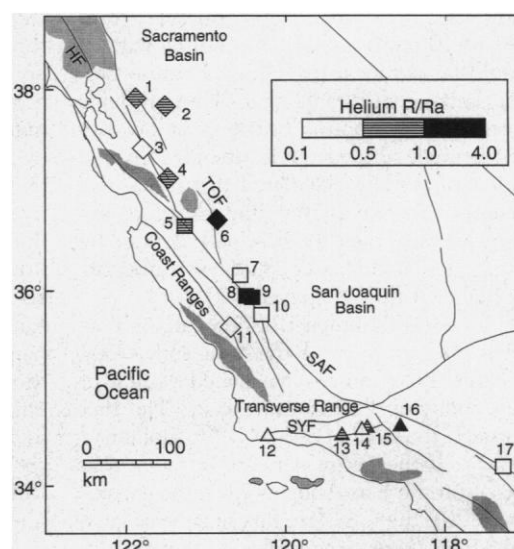


4) but its occurrence is not closely restricted to the main trace of the SAF. The highest ratio (4 Ra, $\sim 50\%$ mantle) was found in Mercey Hot Springs, which emerge from the southern extension of the Tesla-Ortogonalita fault that defines the eastern limit of the central Coast Range. Elevated $^3\text{He}/^4\text{He}$ ratios were also found west of the SAF, although there is a modest trend of decreasing $^3\text{He}/^4\text{He}$ ratios with distance away from the SAF along the Santa Ynez fault in the western Transverse Range (Fig. 3, triangles). These springs are bicarbonate- or sulfate-rich, and the westward decrease in $^3\text{He}/^4\text{He}$ parallels the trend of decreasing CO_2/CH_4 . However, when all samples are considered, there is not a strong correlation between helium isotopes and fluid chemistry, which implies that the influx fluids affect $^3\text{He}/^4\text{He}$ ratios but not other aspects of the fluid chemistry that are controlled by the adjacent crustal provenance lithologies.

Crustal fluids with high $^3\text{He}/^4\text{He}$ ratios have been recognized in regions with active magmatic systems (12) or that are undergoing extension (13). However, aside from some wells with elevated $^3\text{He}/^4\text{He}$ ratios in

New Zealand (14), little data exist for seismically active areas, like the SAF system, that are undergoing compression. A critical question is whether the high $^3\text{He}/^4\text{He}$ fluids represent an active mantle-fed flux or input of residual He from earlier magmatism. Magmatism and development of major volcanic centers followed the northward development of the SAF from 30 to 8 million years ago (15) (Fig. 4). However, because magmas are extensively degassed during emplacement and eruption, resulting in low residual He and high U/He ratios, it is unlikely that the volcanic rocks are a significant source of ^3He or high $^3\text{He}/^4\text{He}$ ratios for circulating fluids. And although magma degassing during emplacement will stain the near-field hydrologic system (16), because of the high U and Th concentrations in local rocks (1 to 5 parts per million) (17), it is also unlikely that stained fluids could retain high $^3\text{He}/^4\text{He}$ ratios (~ 1 to 2 Ra) after 8 to 30 million years of radiogenic ^4He ingrowth (18). Furthermore, the fluid helium isotopic compositions are not correlated with fluid chemistry or related to the age of the local volcanic areas. Thus, the

Fig. 4. California map showing faults associated with the San Andreas system and other regional fault systems (SAF, San Andreas fault; SYF, Santa Ynez fault; TOF, Tesla-Ortogonalita fault; HF, Hayward fault) and the distribution of Tertiary volcanics. Symbol shapes are the same as in Fig. 1 but are shaded in accordance with the helium isotopic composition of the sampled site numbered as follows: 1, Epsom Salt Spring; 2, Byron Springs Well; 3, Alum Rock; 4, Gilroy Hot Spring; 5, Stone Canyon Observation Well; 6, Mercey Hot Springs; 7, Coalinga Mineral Spring; 8, Middle Mountain Oil Well; 9, Varian-Phillips Well; 10, Jack Ranch Highway-46 Well; 11, Paso Robles Spa; 12, Gaviota Warm Spring; 13, Wheeler Hot Spring; 14, Willits Warm Spring; 15, Sespe Hot Spring; 16, Warm Springs; 17, Arrowhead Hot Well.



high $^3\text{He}/^4\text{He}$ ratios represent influx of mantle fluids. The hydrodynamics thus require that (i) the brittle-ductile transition is a permeable boundary and (ii) mantle fluids crossing this boundary and entering the seismogenic zone must be at or near lithostatic pressure.

As mantle fluids flow up through the fault zone, the fluid $^3\text{He}/^4\text{He}$ ratios become diluted with radiogenic ^4He that is produced locally in the crust. This generates a vertical gradient in the helium isotopic composition in the fault zone that depends on the vertical rate of fluid flow and the radiogenic ^4He production rate in the crust. The solution for the integrated upward fluid flow rate (q) for steady-state one-dimensional flow scaled to crustal thickness (19) is

$$q = \frac{H_{\text{crust}} \rho_s P(\text{He})}{\rho_f [^4\text{He}]_{\text{f,mantle}}} \times \left[\frac{(R/Ra)_{\text{meas}} - (R/Ra)_{\text{crust}}}{(R/Ra)_{\text{mantle}} - (R/Ra)_{\text{meas}}} \right] \quad (1)$$

where H_{crust} is the combined thickness of the brittle and ductile crust, ρ_s and ρ_f are the densities of the solid and fluid phases, $P(\text{He})$ is the present day production rate from the U+Th in the fault zone materials, and $(R/Ra)_{\text{mantle,crust,meas}}$ are the helium isotopic compositions in the mantle (8 Ra), produced in the crust (0.02 Ra), and measured in the fault zone fluid. $[^4\text{He}]_{\text{f,mantle}}$ is the initial concentration in the mantle fluid and is calculated from the measured ^4He concentration and helium isotopic composition of the Varian-Phillips well, for which we have the most reliable He concentration data (1.9×10^{-9} mol of ^4He per gram of fluid and 2 Ra), as representative of fault-zone fluids and a crustal thickness (H_{crust}) of 30 km, calculated upward fluid flow rates through the fault zone vary from ~ 1 to 10 mm/year (Fig. 3). The flow rates could be significantly higher, because neither mixing with radiogenic ^4He -rich fluids from the neighboring brittle crust nor hydrodynamic dispersion is included in the calculation. The calculated flow rates also assume continuous flow and therefore are time averages over the flow path defined by H_{crust} ; actual flow rates could be significantly higher if flow is episodic.

To assess the impact of flow rate on possible pressurization of the fault zone, total volatile fluxes must be calculated. A flow of ~ 3 mm/year corresponds to a ^3He flux through the SAF of $\sim 2 \times 10^{-15}$ mol cm^{-2} year $^{-1}$. If the entire network of faults that make up the San Andreas system is considered (20), the total ^3He flux may be as large as ~ 6 mol/year, comparable to that in sev-

eral arc volcanoes (21). One can assume that the mantle ^3He is associated with other more abundant mantle volatiles—certainly CO_2 , and perhaps water. For instance, the upper mantle, as defined by midocean ridge basalts, has a $\text{CO}_2/^3\text{He}$ ratio of $\sim 10^{10}$ (22). The San Andreas system thus may have a CO_2 flux of $\sim 10^{11}$ mol/year.

At seismogenic depths, the density and viscosity of CO_2 are comparable to those of water, and a significant CO_2 flux into the fault zone could help generate and maintain the high pore pressures necessary for fault weakening (9, 23). The pore pressure induced by the CO_2 flux depends on permeability. The permeability of the lower crust is unknown. One extreme is to assume a constant permeability. Then, for a reasonable porosity (0.01) and rock compressibility (10^{-4} MPa $^{-1}$), the ^3He calculated CO_2 flux implies a permeability of $\sim 10^{-21}$ m 2 to maintain high pore pressures through the ductile region and into the seismogenic zone (23). Although this is at the lower end of permeability measured in various rock types, it is probably a lower limit because of the likely addition of nonmantle CO_2 to the system from metamorphic decarbonation reactions in the lower crust. $\text{CO}_2/^3\text{He}$ ratios in most of our samples exceed, at times by >1000 , the mantle value of 10^{10} , and $\delta^{13}\text{C}$ values range from -3 to -15 per mil, indicative of additional nonmantle CO_2 sources. Alternatively, if we assume that permeability decreases exponentially with depth at a rate scaled to a linear increase in stress, then at the base of the seismogenic zone superhydrostatic pressures imply fault zone permeability of $\sim 10^{-18}$ m 2 (9). In this context, fault weakening by mantle fluid inflow at the rate implied by the ^3He flux appears plausible.

We do not know if our sampled features tapped fluids directly from a fault zone or from outside in the adjacent crust. Despite this uncertainty, the flux of mantle He through the system requires a brittle-ductile boundary that is permeable and that supports the fault-weakening model calling for high fluid pressures in the fault zone driven by a mantle source (9). Movement of mantle fluids up through the ductile root zone into the San Andreas system requires that fluid pressures in the lower crust are at lithostatic values and that fluids are directed by the local stress regime in a manner similar to rising magmas (24). If we have sampled fluids directly from fault zones, then the observation that mantle helium is mixed with fluids from the adjacent crust implies that elements of both models (6–9) are important. Because weakness of the fault system is generated by high fluid pressures in the fault zone relative to the surrounding crust, infiltration of crustal fluids

into the fault zone requires episodic reversals of the fluid pressure gradient. Within the seismogenic zone of the fault, local increases in fault-zone porosity induced by fault failure may temporarily lower the fluid pressure, permitting infiltration of crustal fluids (25).

Numerous models for the lithospheric structure of the San Andreas system have been proposed. In some (26), the San Andreas and other major strike-slip faults extend to Moho depths. In others (1, 27), the San Andreas and other faults are limited to the brittle upper crust and sole out into a regional decollement, which may extend as far east as the Sierra Nevada. In the latter models, major faults could tap fluids from an extensive decollement, which in turn might tap mantle fluid sources in regions far removed from the surface expression of the faults. These models may provide a reasonable explanation for the enigmatic ^3He excesses in Mercey Hot Springs and in San Joaquin gas fields (16, 28). A mantle fluid source region extending as far east as the Sierra Nevada is also consistent with recent models for the lack of subcrustal lithosphere beneath the eastern Sierra Nevada (29), and the hypothesized presence of mantle CO_2 in soda springs emerging near the crest of the Sierra Nevada (30).

REFERENCES AND NOTES

1. A. H. Lachenbruch and J. H. Sass, *J. Geophys. Res.* **85**, 6185 (1980).
2. M. D. Zoback *et al.*, *Science* **238**, 1105 (1987).
3. S. Hickman, *Rev. Geophys.* **29**, 759 (1991); S. Hickman, R. Sibson, R. Bruhn, *J. Geophys. Res.* **100**, 12831 (1995).
4. F. A. F. Berry, *Am. Assoc. Petrol. Geol. Bull.* **57**, 1219 (1973); R. H. Sibson, in *Deformation Mechanisms, Rheology and Tectonics*, R. J. Knappe and E. H. Rutter, Eds. (Geological Society, London, 1990), vol. 54, pp. 15–28.
5. P. A. Johnson and T. V. McEvilly, *J. Geophys. Res.* **100**, 12937 (1995).
6. J. D. Byerlee, *Geophys. Res. Lett.* **17**, 2109 (1990).
7. _____, *Geology* **21**, 303 (1993).
8. N. H. Sleep and M. L. Blanpied, *Nature* **359**, 687 (1992).
9. J. R. Rice, in *Fault Mechanics and Transport Properties of Rocks*, B. Evans and T.-F. Wong, Eds. (Academic Press, San Diego, 1992), pp. 475–503.
10. M. Ozima and F. A. Podosek, *Noble Gas Geochemistry* (Cambridge Univ. Press, New York, 1983).
11. $^3\text{He}/^4\text{He}$ ratios have been corrected for air-derived He, which is generally insignificant as shown by $^4\text{He}/^{36}\text{Ar}$ ratios in the samples that are up to ~ 950 times the air ratio.
12. H. Craig, J. E. Lupton, J. A. Welhan, R. Poreda, *Geophys. Res. Lett.* **5**, 897 (1978); B. M. Kennedy, M. A. Lynch, S. P. Smith, J. H. Reynolds, *Geochim. Cosmochim. Acta* **49**, 1251 (1985).
13. E. R. Oxburgh and R. K. O'Nions, *Science* **237**, 1583 (1987).
14. W. F. Giggenbach, Y. Sano, H. Wakita, *Geochim. Cosmochim. Acta* **57**, 3427 (1993).
15. R. B. Cole and A. R. Basu, *Bull. Geol. Soc. Am.* **107**, 167 (1995); W. P. Irwin, in *The San Andreas Fault System, California*, R. E. Wallace, Ed. (U.S. Geological Survey, Washington, DC, 1990), professional paper 1515, p. 61.; R. J. McLaughlin, W. V. Sliter, D. H. Sorg, P. C. Russell, A. M. Sarna-Wojcicki, *Tectonics* **15**, 1 (1996).

16. R. J. Poreda, P. D. Jenden, I. R. Kaplan, H. Craig, *Geochim. Cosmochim. Acta* **50**, 2847 (1986).
17. H. A. Wollenberg, A. R. Smith, E. H. Bailey, *J. Geophys. Res.* **72**, 4139 (1967); F. C. W. Dodge, D. C. Ross, H. A. Wollenberg, A. R. Smith, *Geol. Soc. Am. Abstr.* **1**, 266 (1969).
18. The inability of a stained fluid to retain a residual magmatic signal assumes (i) a mantle He concentration in the stained fluid defined by the measured ^3He content of the Varian-Phillips well (9.52×10^{-16} mol/g), (ii) an initial stained fluid $^3\text{He}/^4\text{He}$ ratio of 8 Ra, (iii) a 5% average porosity, and (iv) a radiogenic ^4He release rate from the host rocks to the stained fluid equivalent to the production rate.
19. T. M. Johnson and D. J. DePaolo, *Water Resour. Res.* **30**, 1571 (1994). Implicit in the steady-state assumption is that the radiogenic ^4He accumulation rate in the fluid is equivalent to the production rate in the host rocks.
20. R. E. Wallace, in *The San Andreas Fault System, California*, R. E. Wallace, Ed. (U.S. Geological Survey, Washington, DC, 1990), professional paper 1515, p. 3.
21. P. Allard, *Geophys. Res. Lett.* **19**, 1479 (1992).
22. B. Marty and A. Jambon, *Earth Planet. Sci. Lett.* **83**, 16 (1987); T. Trull, S. Nadeau, F. Pineau, M. Polve, M. Javoy, *ibid.* **118**, 43 (1993).
23. J. D. Bredehoeft and S. E. Ingebritsen, in *The Role of Fluids in Crustal Processes*, J. D. Bredehoeft and D. L. Norton, Eds. (National Academy Press, Washington, DC, 1990), pp. 158–164.
24. R. C. Bailey, *Geophys. Res. Lett.* **17**, 1129 (1990).
25. P. Segall and J. R. Rice, *J. Geophys. Res.* **100**, 22155 (1995).
26. T. Atwater, *Bull. Geol. Soc. Am.* **81**, 3513 (1970); K. P. Furlong, W. D. Hugo, G. Zandt, *J. Geophys. Res.* **94**, 3100 (1989); J. Namson and T. L. Davis, *Bull. Geol. Soc. Am.* **100**, 257 (1988).
27. D. L. Jones, R. Graymer, C.-Y. Wang, T. V. McEvilly, A. Lomax, *Tectonics* **13**, 561 (1994); B. M. Page and T. M. Brocher, *Geology* **21**, 635 (1993).
28. P. D. Jenden, I. R. Kaplan, R. J. Poreda, H. Craig, *Geochim. Cosmochim. Acta* **52**, 851 (1988).
29. B. Wernicke *et al.*, *Science* **271**, 190 (1996).
30. I. Barnes, R. W. Kistler, R. H. Mariner, T. S. Presser, in *U.S. Geological Survey Water-Supply Paper* (U.S. Geological Survey, Washington, DC, 1981), paper 2181, p. 1.
31. Y. K. Kharaka, F. A. Berry, I. Friedman, *Geochim. Cosmochim. Acta* **37**, 1899 (1973).
32. This work was partly supported by the Director, Office of Energy Research, Office of Basic Energy Sciences, Engineering, and Geosciences Division of the U.S. Department of Energy under contract DE-AC03-76SF00098.

24 January 1997; accepted 14 October 1997

Evolution of the Pacific-Antarctic Ridge South of the Udintsev Fracture Zone

Louis Géli,* Henri Bougault, Daniel Aslanian, Anne Briais, Laure Dosso, Joël Etoubleau, Jean-Pierre Le Formal, Marcia Maia, Hélène Ondréas, Jean-Louis Olivet, Chris Richardson, Keizo Sayanagi, Nobukazu Seama, Anjana Shah, Ivan Vlastelic, Michiko Yamamoto

Because of the proximity of the Euler poles of rotation of the Pacific and Antarctic plates, small variations in plate kinematics are fully recorded in the axial morphology and in the geometry of the Pacific-Antarctic Ridge south of the Udintsev fracture zone. Swath bathymetry and magnetic data show that clockwise rotations of the relative motion between the Pacific and Antarctic plates over the last 6 million years resulted in rift propagation or in the linkage of ridge segments, with transitions from transform faults to giant overlapping spreading centers. This bimodal axial rearrangement has propagated southward for the last 30 to 35 million years, leaving trails on the sea floor along a 1000-kilometer-long V-shaped structure south of the Udintsev fracture zone.

Because of its remoteness, the Pacific-Antarctic ridge (PAR) south of the Udintsev fracture zone (FZ) remained poorly known until the recent past (1). From satellite gravity data, it has been predicted (2) that morphological transitions occur along the ridge axis as the spreading rate increases with distance from the Euler

pole of rotation between the Antarctic and Pacific plates: from 54 mm/year near 65°S up to 74 mm/year at its intersection with the Udintsev FZ, near 55°S (3). Satellite gravity data (4) also reveal a large-scale V-shaped structure that extends for more than 1000 km south of the Udintsev FZ and separates two domains (Fig. 1): one of rough sea floor, with many well-marked fracture zones as is typical of slow spreading centers, and one of smooth sea floor, as is typical of fast spreading centers. Sahabi *et al.* (5) proposed that this V-shaped structure may reflect a change in axial morphology south of the Udintsev FZ that progressively propagated southward during the last 30 million years (My). To analyze this region and test this hypothesis, the French research vessel (R/V) *L'Atalante* (6) explored an 1800-km-long section of the ridge, extending between 65°30'S, 174°40'W and the Udintsev FZ, in January and February of 1996 (Fig. 1).

The PAR south of the Udintsev FZ is

divided into three domains of different morphological signatures (Fig. 2). The southern area, between 65°30'S, 174°40'W and 64°40'S, 172°W, has an axial, valley-type morphology similar to that observed at slow to intermediate spreading centers. The northern area, northeast of 63°10'S, 157°20'W, has an axial, dome-type morphology characteristic of fast spreading centers. In between, a transition zone extends for 800 km along the axis of the PAR.

In the south, the discontinuities separating the 80-km-long segments are curved and resemble overlapping spreading centers (OSCs) (Fig. 2). In the transitional domain, the ridge morphology alternates from a flat axial dome to a shallow axial valley, and most often the across-axis topographic relief is subtle. A large propagating rift (PR) is present near 167°20'W, 63°48'S (Fig. 3) and a second, smaller one near 63°15'S, 165°10'W. Both PRs appear to have initiated at the Heitzler FZ. By extrapolating the pseudofault traces up to this FZ, we estimate that the large PR formed about 2.5 million years ago (Ma), and the younger one about 0.8 Ma. In the northern domain, an axial dome is present at an average depth of 2300 m. However, a rifted high region (near 57°S, for instance) that evolves into an axial graben (south of the 58°20'S OSC, for instance) appears in some places. The ridge axis is offset by three right-lateral transform faults (TFs): the Le Géographe TF near 62°10'S, the L'Astronome TF near 59°30'S, and the Saint-Exupéry TF near 57°30'S (7). The ridge axis is also interrupted by four left-lateral nontransform offsets, three OSCs near 62°30'S, 60°20'S, and 58°20'S, respectively, and one deviation of axial linearity near 57°10'S. Near 61°10'S, a nontransform offset can be inferred from satellite altimetry, but it was not covered during our cruise.

The variation in spreading rate con-

L. Géli, H. Bougault, J. Etoubleau, J.-P. Le Formal, H. Ondréas, J.-L. Olivet, I. Vlastelic, Institut Français de Recherche pour l'Exploitation de la Mer (IFREMER), Boîte Postale 70, 29280 Plouzané, France.

D. Aslanian and C. Richardson, Bullard Laboratories, University of Cambridge, Cambridge, CB30EZ, UK.

A. Briais, Observatoire Midi-Pyrénées, 18 Avenue Edouard Belin, 31055 Toulouse-Cédex, France.

L. Dosso, CNRS-IFREMER, Boîte Postale 70, 29280 Plouzané, France.

M. Maia, Université de Bretagne Occidentale, 6 Avenue Le Gorgeu, 29285 Brest, France.

K. Sayanagi, Geological Survey of Japan, 1-1-3, Higashi, Tsukuba, Ibaraki, 305, Japan.

N. Seama and M. Yamamoto, Chiba University, 1-33, 263 Inage-Bu-Chiba, Chiba, Japan.

A. Shah, School of Oceanography, University of Seattle, Seattle, WA 98195, USA.

*To whom correspondence should be addressed.